Cleat structure analysis and permeability simulation of coal samples based on micro-computed tomography (micro-CT) and scan electron microscopy (SEM) technology

Alexandra Roslin[a], Dubravka Pokrajac[a], Yingfang Zhou[a*]

[a] School of Engineering, University of Aberdeen, Aberdeen, AB243UE, United Kingdom

Abstract

Coal has been playing an important role as a valuable source of energy for many years. In turn, gas production from coal reservoirs is a modern development and coal bed methane (CBM), also known as coal seam gas (CSG), is attracting global attention due to its wide occurrence and benefits for the environment as opposed to the conventional energy sources. Developing coal bed methane reservoirs requires better understanding of the flow behaviours of gas and liquids in cleats and analysis of possible contribution of pores to the flow. This paper describes the implementation of micro computed tomography (micro-CT) and scan electron microscopy (SEM) techniques for analysis of coal samples. Intermediate rank coal samples used in this study were collected from Southern Qinshui Basin (China). In the course of the described research, coal samples were scanned, processed and segmented to study the cleat spacing and permeability. Due to the partial volume effect, the resolution of cleats needed improvement which was achieved by subvoxel processing using a novel algorithm as explained in detail in the paper. Permeability was obtained through simulation of one phase flow using Lattice Boltzmann method (LBM). The results show that the simulated permeability is comparable to the analytical approximation. The subvoxel processing has proved an effective method of overcoming the partial volume effect for the low resolution micro-CT images.

Key words

Coal bed methane; Micro-CT; SEM; Subvoxel algorithm; Permeability; Lattice Botzmann method

1. Introduction

Coal seam gas (CSG), also known as coal bed methane (CBM), is a form of unconventional natural gas extracted from coal reservoirs. Unconventional resources are those hydrocarbon reservoirs whose permeability/viscosity ratio requires use of technology to alter either the rock permeability or the fluid viscosity, or both, in order to produce them at commercially competitive rates. Unlike conventional clastic deposits, coal seams contain a high proportion of mostly localised organic matters in addition to inorganic material. This results in dual-pore system where pores in organic matter are often too small to be efficient flow paths, whereas much larger fractures (known as cleats) are believed to be main conducts from which gas in organic matters can flow out (Clarkson and Bustin, 1996; Moore, 2012; Puri et al., 1991). Developing coal bed methane reservoirs demands better understanding of the flow behaviour of gases and liquids in pores and fractures. This may require the use of sub-micron resolution data for calculation of reservoir petrophysical properties and simulation of gas/water flow behaviour. In turn, the latter demands thorough comprehension of the pore space structure of rocks. Micro-computed tomography and scanning electron microscopy provide an effective source of information on the internal structure of coal porous space.

The evolution of modern micro-CT imaging techniques is based on three-dimensional reconstructions from a series of two-dimensional projections taken at different angles: the sample is rotated and the absorption of X-rays in different directions is recorded and used to produce a three-dimensional representation of the rocks and fluids (Blunt et al., 2013). The main advantage of X –ray micro-computed tomography is that it yields high-resolution three-dimensional images of solid opaque objects quickly and non-destructively (Carlson et al., 2003). It is similar to medical CT scanning, but carried out on a smaller scale and with greatly increased resolution (down to less than 1 micron is possible) (Golab et al., 2013). Implementation of such imaging is of value in a variety of applications, including examination of clastic (Golab et al., 2010; Knackstedt et al., 2010), fractured basement (Knackstedt et al., 2013) and carbonate (Arns et al., 2005) reservoir rocks , as well as three-dimensional studies of coal (Mazumder et al., 2006), paper (Roberts et al., 2003), biomaterials (Knackstedt et al., 2006), bones (Zezabe et al., 2005), volcanic ash (Ersoy et al., 2010), materials for palaeontology (Long et al., 2006), soil science, meteorites, and geotechnics (Ketcham and Carlson, 2001).

In synchrotrons, which were exploited for first micro-CT images of rocks, a bright monochromatic beam of X-ray is shone through a small rock sample (Flannery et al., 1987). The now-standard approach for scanning the pore space of rocks is to use a laboratory instrument, a micro-CT scanner, which houses its own source of X-rays (Arns et al., 2007). The X-rays are polychromatic, and the beam is not collimated – the image resolution is determined primarily by the proximity of the rock samples to the source (Blunt et al., 2013). The intensity recorded for the pixels (2D) and results from reconstruction for the voxels (3D) obtained in micro-CT analysis represents the relative radio density, or relative attenuation of X-rays through individual segments of the imaged material (Novelline, 1997). Within the tomogram, the X-ray opacity of the material in each individual segment determines its brightness, allowing a three-dimensional image to be reconstructed from sections viewed at different angles (Golab et al., 2013). Voids are usually represented as black in micro-CT images due to their low

X-ray opacity, minerals are usually light grey (or white) to medium grey due to intermediate X-ray opacity (Golab et al., 2013).

Many researchers have exploited computed tomography for quantitative characterisation of fractures in coal (e.g. Mazumder et al., 2006; Van Geet and Swennen, 2001 etc.). Other researchers used micro-CT techniques to investigate gas adsorption and desorption in coal (e.g. Karachan and Okandan, 2001), as well as to investigate the heterogeneity and spatial distribution of pores (Giffin et al., 2013), fractures (Yao et al., 2009) and distribution of organic and mineral matter (e.g. Verhelst et al., 1996; Simons et al., 1997) in coals of different rank. The behaviour of fluids in pore space of rocks was extensively examined, but those research studies mostly concentrated on sandstones (Berea sandstone etc.) and carbonates (for example, Estaillades carbonate) (Blunt et al., 2013), with only a few focusing on simulation of gas flow in porous space of coal (e.g. Jing et al., 2016).

In addition to 3D imaging methods, there are other methods, well established in two dimensions, for producing very fine images of rock samples. Amongst them the most widely applied is SEM (scanning electron microscopy) which produces images down to resolution of 10s nm (Blunt et al., 2013). SEM is a technology which generates ultra-high resolution two-dimensional images of thin rock samples (Lemmens et al., 2010). As opposed to micro-CT, this method is destructive, but its advantage is that it allows revealing details of small pores which are beyond the resolution of micro-CT images. SEM images are often used to: provide details which are beyond the resolution of micro-CT images (Golab et al, 2013; Ramandi et al., 2016); calibrate micro-CT images (Mostaghimi et al., 2015); generate synthetic 3D structures from two dimensional thin sections (Wu et al., 2006).

For the purpose of the research described in this paper, micro-CT techniques were used in conjunction with electron microscopy to obtain sufficiently detailed images of intermediate rank coal sample and to segment the cleats of those images. The studied samples are characterised by irregular cleat system which contains mainly thin, poorly resolved fractures due to the partial volume effect. The subvoxel processing algorithm was applied in order to overcome that effect and to improve the quality of the images. The subvoxelled images were then segmented and used for simulating of single-phase flow through the pore space of coal samples. The idea of the subvoxel algorithm was taken from the medical study of trabecular bones (Hwang and Wehrli, 2002) but the algorithm was written for coal and it has never previously been used for rock sample micro-CT images. The study described in this paper concentrated on mm-scale effects. Upscaling of these results to the larger scales was the objective of a follow-up study.

2. Samples and samples preparation

Samples of intermediate rank coal from Panlong mine in Southern Qinshui coal bed methane basin (China) were obtained and examined, the samples are buried in a range of 600-750 meters subsurface and in this work one sample (Figure 1) was chosen in order to analyse cleat porosity and permeability. The main characteristics of the analysed coal sample acquired from coal proximate analysis are listed in Table 1.

Figure 1. Coal core sample in a sample holder used in this study.

Table 1. Coal sample characteristics.

Sample ID	Sample (%)			Organic matter (%)			Vitrinite Reflectance^{o} $_{ran}$ (%)
	Organic matter	Pyrite	Others	Vitrinite	Inertinite	Liptinite	
PL3#-2	79.87	0.17	19.97	77.52	22.48	0.00	1.68

Previous studies (e.g. Wang et al., 2016; Cai et al., 2011) show that the coal from this basin contain 0.59 – 3.54% moisture, 3.5 – 15.54% ash yield, 73.62 – 88.92% fixed carbon and 2.14 – 4.04% hydrogen, with C/H ratios in the range of 19.96 – 36.25. The vitrinite reflectance ranges from 1.95 to 3.49%, with 18.5 – 97.4% vitrinite and 2.4 – 81.4% inertinite. The gas in-place concentration is in the range from 0.72 to 2.88x10^{8} m^{3}/km^{2}, with an average of 1.21x10^{8} m^{3}/km^{2}.

Samples were not dried or saturated with any high contrast fluid to preserve samples integrity. For SEM analysis, the sample surface was polished in three different directions and carbon-coated (see Figure 2).

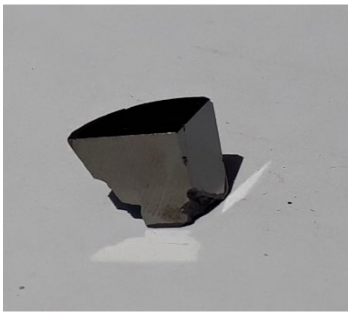

Figure 2. Coal core sample polished and carbon-coated for SEM analysis.

3. Methodology

X-ray micro-computed tomography was conducted using the laboratory-based ZEISS VersaXRM-410 3D microscope (Figure 3), which delivers non-destructive 3D imaging with submicron resolution, for in situ scanning, and provides high-resolution micro-CT images for the widest range of sample sizes. This machine uses patented detectors which convert X-rays into visible light and then uses a microscope turret of objectives for easy and accurate zooming. VersaXRM-410 achieves 0.9 µm true spatial resolution with minimum achievable voxel size of 100 nm. Advanced absorption and phase contrast (for soft or low-Z materials) provide greater versatility in overcoming the limitations of traditional computed tomography (CT).

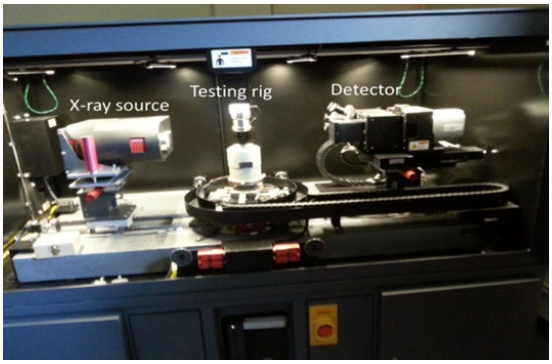

Figure 3. ZEISS XRadia 410 Versa microscope (Kartal et al., 2017).

The first scan was done at the resolution of 25 microns to understand the internal structure of coal. This scan was run at an X-ray beam energy of 80 kV and a power of 10 W. The distance between the specimen and X-ray source was 57.024 mm while there was 97.76 mm between the specimen and detector. An optical magnification of 0.4X was used to achieve high resolution. This gave a 25-micron pixel size and exposure time was set to 1.2 s in order to get intensity values for the best signal-to-noise ratio for each projection (radiograph). The next scan was done to achieve the resolution of 10 micron to focus on the most vitrinite half of the sample. The scan parameters for all samples are summarised in the Table 2. Having analysed 25- and 10-micron slides, the areas of interest were chosen, and four 2.5-micron slides were chosen with the most representative volume for porosity analysis and flow simulation.

Table 2. Micro-CT scanning parameters.

Sample	Resolution, micron	Voltage, kV	Power, W	Distance to source, mm	Distance to detector, mm	Optical magnification	Exposure time, s
PL3#-2	25	80	10	57.0	97.8	0.4	1.2
PL3#-2	10	80	10	60.0	326.2	0.4	10
PL3#-2	2.5	120	10	65.0	110.0	4	15
PL3#-2	2.5	120	10	65.0	110.0	4	15
PL3#-2	2.5	120	10	65.0	110.0	4	15
PL3#-2	2.5	120	10	65.0	110.0	4	16

Scanning electron microscopy technique was also exploited during the research but only of the upper surface of each sample at this stage. These SEM images were initially used for visual analysis of the width, integrity and mineralisation of the fractures to understand which parts of the sample should be targeted for scanning. Later, the samples were cut, and a few thin sections were prepared for further SEM analysis. Because the thin sections were extracted from different parts of the samples (not only from the surface) there will be an opportunity to calibrate micro-CT images with SEM data. The SEM images were obtained with magnification 22, 27 or 29, 100, 150, 250, 300 and 350 depending on the samples and the size of the features to be evaluated.

4. Results

Grid independence test

Prior to calculating permeability of coal samples a grid independence test was carried out to validate the simulation method, and to find the best resolution for a sufficiently accurate numerical simulation. The test compared measured flow through a single fracture with constant width (defined by the average fracture width in the studied sample determined from 2.5-micron scanned and 2.5-micron subvoxelled images) to the analytical solution. The fracture width was 25 microns, and the simulations were run for the following resolutions of the numerical grid: 2, 5, 10, 25 and 50 cells per fracture width (i.e. 12.5, 5, 2.5, 1 and 0.5 micron cell size, respectively). The comparison of the velocity profiles across the fracture with analytical solution is shown in Figure 4. It was observed that for resolutions coarser than 10 cells per fracture width, there was a big discrepancy between analytical and numerical solutions. At the same time, the most accurate resolution was 50 cells per fracture width, as expected (Figure 4). Resolutions 25 and 10 cells per fracture width show 15% and 18% discrepancy respectively, which was considered sufficiently accurate for the purpose of the study.

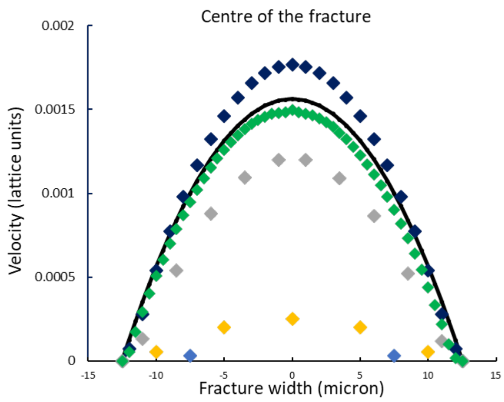

Figure 4. Velocity profile across the fracture width: analytical solution (continuous black line) and numerical solution for different grid resolution (coloured symbols): blue – 2 cells per fracture width; yellow – 5 cells per fracture width; grey – 10 cells per fracture width; dark blue – 25 cells per fracture width; green – 50 cells per fracture width.

Subvoxel processing and segmentation

After micro-CT scans were obtained, images were processed and analysed versus SEM data, and it was found that the resolution of cleats is quite poor due to the partial volume effect, and the width of the cleats is overestimated for 25-, 10- and 5-micron scans compared to the width obtained from SEM images (25 microns determined from SEM and 100 microns determined from 10-micron micro-CT scans). On the other hand, the discrepancy between the widths of the cleats obtained from SEM and 2.5-micron micro-CT scans is about 1-2 micron. After couple unsuccessful attempts to improve the resolution of cleats by application of different segmentation methods, the subvoxel processing algorithm was written and implemented in Matlab to overcome the partial volume effect. After analysis of SEM data and performing the grid dependence tests, we concluded that 2.5-micron resolution appears to be the best solution for the studied samples. The problem of scanning samples at 2.5-micron resolution is that the volume of investigation in case of this resolution is reduced to 2.5mm*2.5mm*2.5mm which was not sufficiently large to be representative. Collecting series of separate volumes at 2.5-micron could have been a solution but it was difficult due to the scanning time and expenses. Thus, it was decided to take 10-micron images and improve the resolution of these images by subvoxel processing.

The idea to use subvoxel processing was taken from medicine (Hwang and Wehrli, 2002) and is supposed to be applicable to volumes of interest containing materials or phases with two discrete signal intensities (coal matrix and cleats in the case of current research). The principal strategy consists of subdividing voxels and assigning voxel intensities to each subvoxel on the basis of local neighbourhood criteria.

However, the approach to subvoxel processing was adapted and the algorithm was written to be applicable for coal samples gray-scale images. Thus, the starting point of the algorithm for trabecular bones images was the partitioning of each voxel into eight subvoxels by strictly enforcing conservation of bone mass (Hwang and Wehrli, 2002). In order to ensure bone mass conservation, Hwang and Wehrli (1999) generated bone volume fraction to determine the spatial distribution of trabecular bone. In the current research, the subvoxel processing was performed directly on the gray-scale images (where each voxel has a value from 0 to 255) and the restrictions to the algorithm were as follows: 1) the average sum of eight subvoxels values should be equal to the value of the original voxel, and 2) each subvoxel value could not exceed 255. Also, for trabecular bones images, each neighbouring pixel had the same contribution but if the resulting subvoxel was next to the voxels with zero BVF, this subvoxel was zeroed. With the current research, the following scheme was used: each voxel was partitioned into eight voxels (1, 2, 3, … 8 in Figure 5) and the resulting subvoxels were assigned the gray-scale intensity values based on the intensity values of neighbouring voxels, considering the proximity of each neighbour. Each subvoxel has 7 neighbours (for instance green, yellow and red voxels shown in Figure 5 are the neighbours of the subvoxel 1): with 3 of them (green in Figure 5) it has face-face connection, with 3 of them (yellow in Figure 5) – edge-edge connection and with 1 of them (red in Figure 5) – point-point connection. The weight of each neighbouring voxel is calculated based on the proximity to the subvoxel of interest: the weight of neighbouring voxels with face-face connection is 25%, with edge-edge connection – 8% and with point-point connection – 1%. Subvoxel processing is an empirical algorithm rather than one derived from mathematical theory (Hwang and Wehrli, 2002), so the optimal weighed contribution of each neighbouring voxel was determined by trying different configurations and comparing the subvoxelled images to the images scanned with higher resolution.

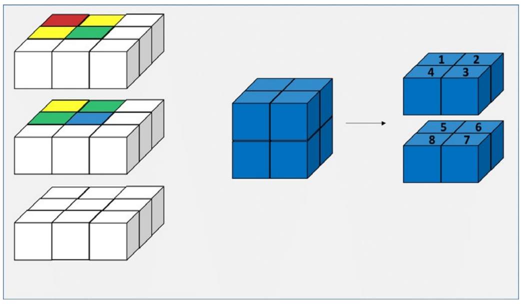

Figure 5. Subvoxel partitioning scheme in 3D.

For the purpose of this research, the same volume of coal sample was scanned with different resolutions – 10-, 5- and 2.5-microns. Then, subvoxel processing was performed on 10-micron images a couple of times with different weighed contribution of neighbouring pixels (starting from equal weight of all neighbours and continuing towards an increase of contribution of face-face neighbours) and after each iteration, the results were compared to the scanned 5-micron images, and when the optimal result was achieved, subvoxel processing was repeated on subvoxelled images to achieve 2.5-resolution. Then, the resulting 2.5-subvoxelled images were compared to scanned 2.5-micron images for quality control. Images were compared in the following manner: the same features (similar intervals of cleats) were chosen on 5- and 2.5-micron scanned image and the width of cleats was determined by comparison with the one determined from SEM images. This calibrated width was then compared to the width of the same features obtained from 5- and 2.5-micron subvoxelled images. The results of subvoxel processing was accepted as optimal when the discrepancy between the width of analysed cleats was about 1-2 micron (less than 10% of the width). As a result of application of this method, the resolution of cleats was improved (Figure 6) but the volume of investigation of new 2.5-micron subvoxelled images is 64 times bigger than that of 2.5-micron scanned images.

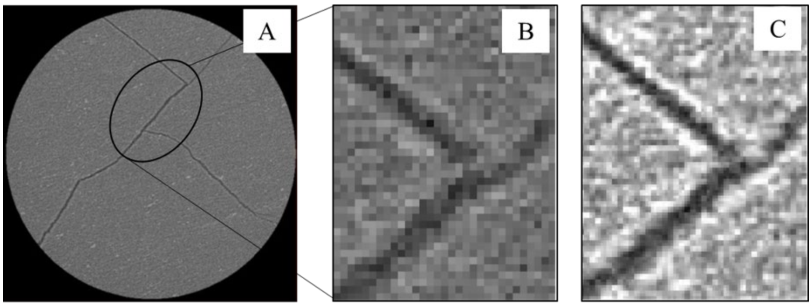

Figure 6. An example of subvoxel processing results: A) 2.5-micron scanned image; B) 10-micron image before processing; C) 10-micron image after processing to 2.5-micron subvoxelled image.

The next step of micro-CT scans analysis was image segmentation. Based on the experience of previous researchers, the Ramandi et al., 2016 watershed method was chosen for image segmentation. This approach was successfully applied by Ramandi et al. for Australian coal samples, but used a combination of dry and wet coal images for better contrast between fractures and coal matrix. In the course of the current research coal was not saturated with any contrast fluid, and as a result of this, some unwanted noise appeared on segmented images which had to be removed by different filters. The most effective filter for the studies samples was median filter (Figure 7).

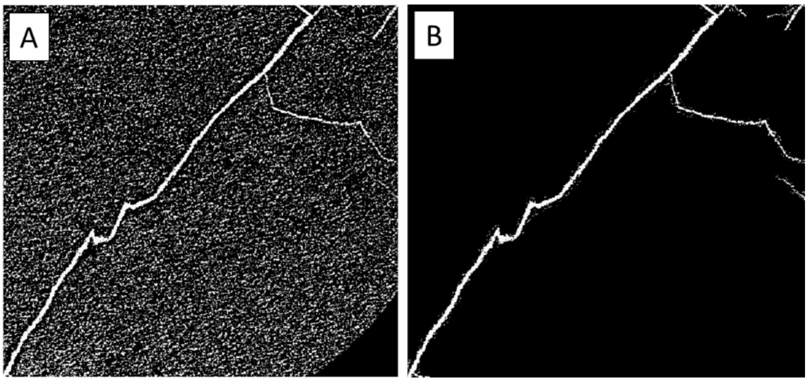

Figure 7. The results of watershed- method segmentation in 2D and 3D – black is coal matrix, light colour – cleat: A) before noise removal; B) after noise removal.

Permeability simulation using LBM

Permeability of coal samples was determined from numerical simulations of steady state single-phase flow through the samples. Simulations were performed using Palabos, which is an open-source computational fluid dynamics (CFD) solver based on the Lattice Boltzmann method. The Lattice Boltzmann method (LBM) is one of a number of particle-based CFD methods, where particles representing packets of fluid are tracked through the computational domain (Blunt et al., 2013).

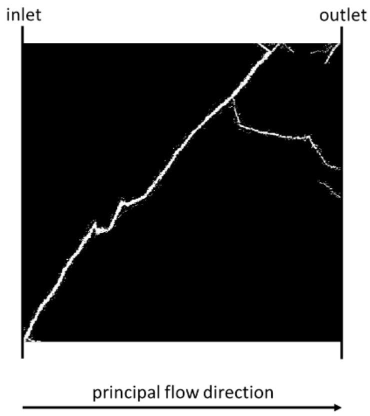

Figure 8. An example of flow domain (2.5-micron scanned set) – the size of the sides is 2.5*2.5 mm.

Permeability simulation was performed on three different sets of images: 10-micron scanned, 2.5-micron scanned and 2.5-micron subvoxelled (Figure 8) to compare the results and estimate the sensitivity of permeability simulation to scanning resolution. For the simulation the following parameters were used: the D3Q19 lattice, bounce-back boundary conditions at the solid boundaries (walls), and a fixed pressure difference between the inlet and the outlet. A simulation starts with fluid having zero velocity, and with a constant pressure gradient in the x-direction (i.e. the principal flow direction). The permeability was computed by applying Darcy's law to the simulated velocity data，

$$k = U\mu \frac{dx}{dp} \qquad (1)$$

here U is average velocity in x-direction in the cleat, μ is the fluid viscosity and $\frac{dp}{dx}$ is the pressure gradient along the principal flow direction (i.e. between the inlet and outlet).

Since reconstruction of 3D geometry can produce slightly different results depending on the value of threshold applied in the segmentation process, for each set of images listed above, permeability simulation was performed several times. Table 3 summarises simulated permeability results according to the different thresholds used in segmentation process: in the course of each image set segmentation, three different points on each intensity histogram were chosen for watershed segmentation, and the resulted images were used for simulation. To sum all, the following results were obtained: permeability was determined in the range 75-125mD for 2.5-micron subvoxelled images, in the range 125-205mD for 2.5-micron scanned images, in the range 2400-3000mD for 10-micron scanned images.

Table 3. Simulated permeability results depending on segmentation thresholds.

	Image set		
Threshold point on histogram	2.5 scanned	2.5 subvoxelled	10 scanned
25%	125 mD	75 mD	2400 mD
50%	152 mD	88 mD	2670 mD
75%	205 mD	125 mD	3000 mD

For the purpose of analytical solution, the fractures are assumed to have constant aperture *d*, to be parallel to the principal flow direction and to be at equal distances *s*, such that porosity of this system ϕ, is equal to the ratio d / s. Based on the analytical solution for Poiselle flow between parallel plates the permeability of such system is:

$$k = \frac{\phi d^2}{12} \qquad (2)$$

Previous researchers (e.g. Oron and Berkowitz, 1998) claimed that fracture aperture should be measured as an average over a certain length. Analysis of SEM and micro-CT images of the samples used in this research showed that coal fractures of studied samples are quite constant and consistent in width (see Figure 8), so it was decided to use average fracture aperture measured perpendicular to the main axis of fractures. Thus, analytical solution for the average fracture width (determined from 2.5-micron scanned and 2.5-micron subvoxelled images) gave the value of 82.5mD which is comparable with numerical simulation results.

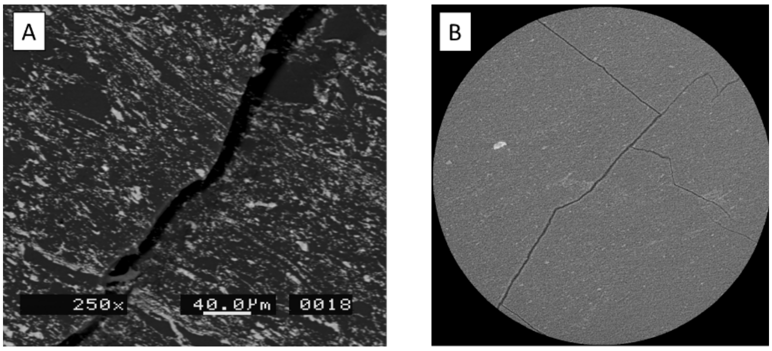

Figure 8. SEM image (A) and micro-CT image (B) demonstrate that the fracture width is quite constant

5. Discussion, conclusion and future challenges

The research described in this paper focuses on implementation of micro-CT and SEM technologies for analysis of coal including improvement of image resolution, and the sample from Southern Qinshui Basin (China) was exploited for the research. It was observed that this coal was characterised by irregular cleat system which contained mainly thin fractures. This had two consequences: 1) poor resolution of those fractures due to the partial volume effect at lower resolutions (10- and 25-micron); 2) at higher resolution the scanned volume was too small to be representative of cleat system of those samples. Taking into account these two considerations, it was decided to use subvoxel processing algorithm to increase the resolution of 10-micron images to 2.5-micron but keeping volume of investigation of 10-micron images. This method was proven on 10-micron images but also later tested on different images with resolution from 25 to 2 microns. The idea for this approach was taken from medicine, but the approach was adapted to the area of the research and the algorithm was written based on the studied coal samples. The method was proved to overcome the partial volume effect, as long as cleat width is larger than the pixel size of a scan. It was also observed that there is no value in subvoxel processing below 2-micron resolution as it doesn't improve much the resolution of cleats. The establishing of subvoxel algorithm was utterly important for the current research as this algorithm allowed the authors to analyse coal thin features but significantly reduced the scanning time due to bigger volume of investigation of each scan.

The problem of optimal resolution required for permeability simulation, which provides a good balance between accuracy and efficiency, was also investigated in the course of this research. It was found that the resolution that provides the most accurate permeability simulation (1.5% discrepancy with analytical solution) is 50 cells per fracture, which equates to 0.5-micron resolution. The minimal resolution for reasonably accurate simulation is 10 cells per fracture or 2.5 micron (18% discrepancy with analytical solution). In the future, 2.5-micron resolution will be used as a standard to work with these samples.

In the course of this research, the permeability simulation was also performed on different images (with different resolution) and compared with analytical solution for Poiseulle flow in a single crack. Permeability simulation was performed for two reasons: 1) it was required for validation of the results of image subvoxelling and segmentation, and 2) the results obtained on mm-scale will further be used to upscale permeability to cm-scale. Numerical simulation demonstrated that the permeability simulated on 2.5-micron scanned images is in accordance with the permeability obtained for 2.5-micron subvoxelled images (125-205mD and 75-125mD correspondingly), while 10-micron scanned images gave the permeability in the range 2400-3000mD. Considering that the analytical solution for an average fracture width gives permeability 82.5mD, it was concluded that simulation for 10-micron scans greatly overestimated permeability. The latter supports the observation that the width of cleats determined from 10-micron scanned images was also overestimated compared to the one obtained from SEM data. However, the permeability obtained from the simulation is greater than the expected from the analysis of coal samples from the studied coal basin. This was probably due to the scale effect, i.e. to the fact that only a limited volume of coal was used for simulation. Moreover, this volume contained a couple of fractures with considerable width, which increased the porosity of the sample up to 4%. Analysis of the whole sample shows that the cleat porosity of the sample was lower (about 1.8%). Laboratory measurements of permeability of studied coal samples are in progress at the moment but available data from the studied basin show that coal permeability is in the range 0.01-0.37mD (Li et al., 2016).

The research described in this paper was performed at mm-scale and the problem of upscaling permeability data to get permeability for the whole sample, as well as the validation of upscaling, is not discussed in this paper. One possible way of addressing this challenge is to identify the key features from rock images, e.g., self-similar behaviour (Wu, et al., 2019), which control the flow behaviour at different scale and then apply the feature based approach (Singh and Cai, 2018a; 2018b) to estimate the permeability at different scale. Finally, it must be noted that the research described in this paper considered only cleat porosity and permeability. Pore matrix porosity will be investigated at the next stage of the research.

Acknowledgment

This paper utilised opportunistic coal samples and characterisation data as a part of a study into multiphase flow in coal for Southern Qinshui coal basin. The University of Aberdeen School of

Engineering and School of Geosciences are thanked for their support. The authors also thank John Still from The University of Aberdeen School of Geosciences for his support regarding SEM data analysis and Amir Golparvar from The University of Aberdeen School of Engineering for his help with Matlab.

References

1. Arns C.H., Bauget F., Limaye A., Sakellariou A., Senden T.J., Sheppard A.P., Sok R.M., Pinczewski W.V., Bakke S., Berge L.I., Oren P.E., Knackstedt M.A., 2005. Pore-scale characterization of carbonates using X-ray microtomography. SPE Journal, 10 (4), 475–84.
2. Arns J.Y., Sheppard A.P., Arns C.H., Knackstedt M.A., Yelkhovsky A., Pinczewski W.V., 2007. Pore-level validation of representative pore networks obtained from micro-CT images. In: Proceedings of the annual symposium of the society of core analysis, SCA 2007-A26, Calgary, Canada.
3. Blunt M.J., Bijeljic B., Dong H., Gharbi O., Iglauer S., Mostaghimi P., Paluszny A., Penland C., 2013. Pore-scale imaging and modelling. Advanced in Water Resources, 51, 197-216.
4. Cai, Y., Liu, D., Yao, Y., Li, J., Qiu, Y., 2011. Geological controls on prediction of coalbed methane of No. 3 coal seam in Southern Qinshui Basin, North China. International Journal of Coal Geology, 88, 101 – 112.
5. Carlson, W.D., Rowe, T., Ketcham, R.A., Colbert, M.W., 2003. Applications of high resolution X-ray computed tomography in petrology, meteoritics and paleontology. In: Mees, F., Swennen, R., Van Geet, M., Jacobs, P. (Eds.), Applications of X-ray Computed Tomography in the Geosciences: Geological Society, London, Special Publication, 215, 7–22.
6. Clarkson, C.R., Bustin, R.M., 1996. Variation in micropore capacity and size distribution with composition in bituminous coal of the Western Canadian Sedimentary Basin: implications for coalbed methane potential. Fuel, 75, 1483–1498.
7. Ersoy, O., Şen, E., Aydar, E., Tatar, İ., Çelik, H.H., 2010. Surface area and volume measurements of volcanic ash particles using micro-computed tomography (micro-CT): a comparison with scanning electron microscope (SEM) stereoscopic imaging and geometric considerations. Journal of Volcanology and Geothermal Research, 196, 281–286.
8. Flannery, B.P., Deckman H.W., Roberge W.G., D'Amico K.L., 1987. Three-dimensional X-ray microtomography. Science, 237, 1439–1444.
9. Giffin, S., Littke, R., Klaver, J., Urai, J.L., 2013. Application of BIB-SEM technology to characterise macropore morphology in coal. International Journal of Coal Geology, 114, 85-95.
10. Golab, A., Knackstedt, M.A., Averdunk, H., Senden, T., Butcher, A.R., Jaime, P., 2010. 3D porosity and mineralogy characterization in tight gas sandstones. The Leading Edge, 936–942 (December).

11. Golab A., Ward C.R., Permana A.,Lennox P., Botha P., 2013. High-resolution three-dimensional imaging of coal using microfocus X-ray computed tomography, with special reference to modes of mineral occurrence. International Journal of Coal Geology, 113, 97-118.
12. Hwang S.N., Wehrli F.W, 1999. Estimating voxel volume fractions of trabecular bone on the basis of magnetic resonance images acquired in vivo. International Journal of Imaging Systems and Technology, 10, 186–198.
13. Hwang, S.N., Wehrli, F.W., 2002. Subvoxel processing: a method for reducing partial volume blurring with application to in vivo MR images of trabecular bone.
14. Jing, Y., Armstrong, R.T., Ramandi, H.L., Mostaghimi, P., 2016. Coal cleat reconstruction using micro-computed tomography imaging. Fuel, 181, 286 – 299.
15. Karachan, C.O., Okandan, E., 2001. Adsorption and gas transport in coal microstructure: investigation and evaluation by quantitative X-ray CT imaging. Fuel, 80, 509-520.
16. Kartal, M., Dugdale, L.H., Harrigan, J.J., Siddiq, M., Pokrajac, D., Mulvihill, D.M., 2017. Three-dimensional in situ observations of compressive damage mechanisms in syntactic foam using X-ray microcomputed tomography. Journal of Materials Science, 52, 10186-10197.
17. Ketcham R.A., Carlson W.D., 2001. Acquisition, optimization and interpretation of X-ray computed tomographic imagery: applications to the geosciences. Computers & Geosciences, 27, 381–400.
18. Knackstedt, M., Arns, C., Senden, T.J., Gross, K., 2006. Structure and properties of clinical coralline implants measured via 3D imaging and analysis. Biomaterials, 27 (13), 2776–2786.
19. Knackstedt, M., Jaime, P., Butcher, A.R., Botha, P.W.S.K., Middleton, J., Sok, R., 2010. Integrating reservoir characterization: 3D dynamic, petrophysical and geological description of reservoir facies. In: Proceedings of the SPE Asia Pacific oil and gas conference and exhibition, 18–20 October, 2010, Brisbane, Queensland, Australia, SPE 133981.
20. Knackstedt, M., Carnerup, A., Golab, A., Sok, R., Young, B., & Riepe, L., 2013. Petrophysical Characterization of Unconventional Reservoir Core at Multiple Scales. Society of Petrophysicists and Well-Log Analysts, 54 (03).
21. Lemmens H.J., Butcher A.R., Botha P.W.S.K., 2010. FIB/SEM and automated mineralogy for core and cuttings analysis. In: Proceedings of the SPE Russian oil and gas conference and exhibition, 26–28 October, 2010, Moscow, Russia, SPE 136327.
22. Li, C., Liu, D., Cai, Y., Yao, Y., 2016. Fracture permeability evaluation of a coal reservoir using geophysical logging: a case study in the Zhengzhuang area, southern Quishui Basin. Energy Exploration and Exploitation, 34 (3), 378–399.
23. Long, J., Young, G., Holland, T., Senden, T., Fitzgerald, E., 2006. An exceptional Devonian fish from Australia sheds light on tetrapod origins. Nature, 444, 199–202.

24. Mazumder, S., Wolf, K.-H.A.A., Elewaut, K., Ephrain, R., 2006. Application of X-ray computed tomography for analyzing cleat spacing and cleat aperture in coal samples. International Journal of Coal Geology, 68, 205–222.
25. Moore, T.A., 2012. Coalbed methane: a review. International Journal of Coal Geology, 101, 36 – 81.
26. Mostaghimi, P., Armstrong, R.T., Gerami, A., et al., 2015. Micro-CT imaging and microfluidics for understanding flow in coal seam reservoirs. Paper presented at the International Symposium of the Society of Core Analysts, Newfoundland, Canada, 16–21 August.
27. Novelline, R., 1997. Squire's Fundamentals of Radiology. Harvard University Press, Cambridge, Massachusetts, 638.
28. Puri, R., Evanoff, J., Brugler, M., 1991. Measurement of coal cleat porosity and relative permeability characteristics. Paper presented at the SPE Gas Technology Symposium, Houston, Texas.
29. Ramandi H. L., Mostaghimi P., Armstrong R.T., Pinczewski W.V., 2016. Porosity and permeability characterization of coal: A micro-computed tomography study. International Journal of Coal Geology, 154-155, 57-68.
30. Roberts, R., Senden, T.J., Knackstedt, M.A., Lyne, M.B., 2003. Spreading of aqueous liquids in unsized papers is by film flow. Journal of Pulp and Paper Science, 29, 123–130.
31. Singh, H. and Cai, J., 2018a. A Feature-Based Stochastic Permeability of Shale: Part 1—Validation and Two-Phase Permeability in a Utica Shale Sample. Transport in Porous Media 126 (3), 527–560.
32. Singh, H. and Cai, J., 2018b. A Feature-Based Stochastic Permeability of Shale: Part 2-Predicting Field-Scale Permeability. Transport in Porous Media 126 (3), 561-578.
33. Simons, F.J., Verhelst, F., Swennen, R., 1997. Quantitative characterization of coal be means of microfocal X-ray computed microtomography (CMT) and colour image analysis (CIA). International Journal of Coal Geology, 34, 69-88.
34. Van Geet, M., Swennen, R., 2001. Quantitative 3D-fracture analysis by means of microfocus X-ray computer tomography (micro-CT): an example from coal. Geophysical research letters, 28 (17), 3333-3336.
35. Verhelst, F., David, P., Fermont, W., Jegers, L., Vervoort, A., 1996. Correlation of 3D-computerised tomographic scans and 2D-colour image analysis of Westphalian coal by means of multivariate statistics. International Journal of Coal Geology, 29, 1-21.
36. Wang, H., Yao, Y., Liu, D., Pan, Z., Yang, Y., Cai, Y., 2016. Fault-sealing capability and its impact on coalbed methane distribution in the Zhengzhuang field, southern Quinshui Basin, North China. Journal of Natural Gac Science and Engineering, 28, 613 – 625.

37. Wu, H., Zhou, Y., Yao, Y. and Liu, D., Imaged based fractal characterization of micro-pore structure in coal sample, Fuel 239, 53-62.
38. Wu K., Van Dijke M.I.J., Couples G.D., Sorbie K.S., Ma J., 2006. 3D stochastic modelling of heterogeneous porous media – applications to reservoir rocks. Transport Porous Media, 65 (3), 443–67.
39. Yao, Y., Liu, D., Che, Y., Tang, D., Tang, S., Huang, W., 2009. Non-destructive characterization of coal samples from China using microfocus X-ray computed tomography. International Journal of Coal Geology, 80, 113-123.
40. Zezabe, R., Jones, A., Knackstedt, M., Seeman, E., 2005. Femoral neck shape and the spatial distribution of its mineral mass varies with its size: clinical and biomechanical implications. Bone, 37 (2), 243–252.